ESTIMATING STRENGTH OF LATTICE STRUCTURE USING MATERIAL EXTRUSION BASED ON DEPOSITION MODELING AND FRACTURE MECHANICS

Sang-in Park *, †, Narumi Watanabe **, David W. Rosen *, †

*G.W.W. School of Mechanical Engineering, Georgia Institute of Technology, Atlanta, GA
** The Boeing Company, Seattle, WA
†Singapore University of Design and Technology, Singapore

Abstract

Geometrical complexity in lattice structures yields large bounding surfaces to be approximated during additive manufacturing (AM) processes. In material extrusion, approximation of geometries using finite-sized thin filaments introduces defects such as voids and gaps in as-fabricated geometries. This initiates cracks between layers and increases possibility of fracture by crack propagation. As a result, a lattice structure fabricated by material extrusion tends to fail at significantly lower stress than estimated strength without consideration of fracture mechanism. The goal of this research is to estimate strength of material extruded lattice structures considering bonding strength among layers. To achieve this, the bonding strength is determined based on a deposition process modeling scheme and fracture mechanics analysis. A two-layer deposition model is generated to investigate deposited geometry, and the effective interlayer-bonding strength is calculated using a cohesive zone model (CZM) and peel tests. The resulting strength is incorporated into the property-estimation procedure.

Introduction

Additive manufacturing process provides new opportunities to design and manufacture geometrically complex parts such as lattice structures and cellular materials. Recent advances in additive manufacturing process have been improving geometrical accuracy and mechanical properties of as-manufactured parts. However, geometrical approximation occurred in additive manufacturing processes still yields geometrical degradation [1, 2]. In particular, the geometrical degradation becomes more critical in lightweight lattice structures composed of many thin elements like bars and beams, since the structures have large bounding surfaces, which increase possibility of geometrical degradation [3]. In material extrusion processes, thin filaments are deposited along deposition paths to approximate geometries in a building plane. Since the filaments have finite size and elliptical or circular cross sections, voids and gaps shown in Figure 1 are formed between filaments during manufacturing. The process-induced voids and gaps initiate cracks in fabricated parts in the building plane as well as along the building direction. These cracks limit mechanical strength of fabricated parts as they grow along filament interfaces or layer surfaces. Furthermore, voids and gaps may have larger influence on strength of lattice structure than bulky parts, since lattice structures are composed of thin members of which the size is several times of the filament diameter. Thus, crack propagation more easily degrades strength of lattice structures than bulky parts.

Many researchers have investigated degradation in mechanical properties of additively manufactured parts. Ahn et al. reported material anisotropy depending on deposition patterns in material extrusion processes [4]. In the research, significant strength drop was observed when a raster angle is perpendicular to an external force direction. Rodriguez et al. investigated a relationship between a raster angle of deposition path and tensile strength [5]. The authors addressed that the raster angle has a large influence on strength, and they proposed a design framework for improving mechanical properties of material extruded parts by optimizing raster angles. Bagsik and Schöppner measured tensile strength of additively manufactured specimens, which are built in three building directions [6]. This research also reported large reduction in strength over 40% for vertically built specimens.

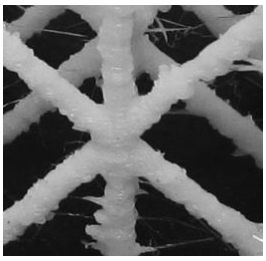

(a) Stair steps [2]

(b) Voids and gaps

Figure 1 Geometrical degradation in material extrusion processes

Researchers have implemented fracture mechanics to understand the material anisotropy and strength reduction shown in additively manufactured parts. Thomas and Rodriguez investigated wetting and thermally driven diffusion bonding processes to estimates fracture toughness between two deposition lines [7]. The authors performed two dimensional heat transfer analysis to capture temperature distribution during solidification process in material extrusion process and analytically derived fracture toughness between deposition lines. Fracture mechanics approach recently receives more attentions. Young et al. proposed an experimental procedure to measure interlayer fracture toughness in additively manufactured parts [8]. The authors modified a standard double cantilever beam (DCB) specimens in order to apply to additively manufactured specimens. Gardan et al. developed a design framework to improve fracture toughness based on the direction of principle stresses and demonstrated more durable deposition path pattern against crack propagation [9]. Kishore et al. devised an infrared preheating system to enhance the interlayer fracture strength of parts manufactured in a material extrusion based big area additive manufacturing (BAAM) machine [10]. Seppala et al. investigated interlayer bonding strength based on isothermal healing time in polymer-polymer welding process [11]. Research related to fracture mechanics in additive manufacturing research area has focused on experimental procedure.

Cohesive zone model (CZM) is a numerical fracture analysis model devised to describe crack propagation and fracture in bonded interfaces [12-14]. Several researchers recently have implemented the numerical scheme to study interlayer fracture and to investigate strength of additively manufactured parts. Liravi et al. developed a cohesive zone model to estimate a pulling-up force at failure in a bottom-up projection-based photo polymerization process [15]. Spackman et al. constructed CZM and proposed model-based design framework for a fiber-reinforced soft composite additive manufacturing process. [16] The authors selected CZM parameters based on calibration experiments. Ahmadi et al. implemented CZM to assess mechanical properties of metal parts fabricated by a powder bed fusion process [17]. The authors utilized CZM to define interactions among melt pool boundaries based on their observation that melt pool boundaries are weaker than grain boundaries so that defects are initiated in melt pool boundaries. They predicted effects of microstructure on mechanical properties of fabricated parts based on numerical analysis with CZM.

In material extrusion processes, fracture mechanics approach can be used to explain strength degradation between layers or deposition paths. However, previous research has focused on experimental aspects of the approach. Constructing a numerical fracture mechanics model can help to expedite design processes utilizing material extrusion processes by providing a systematic analysis framework. The goal of this research is to estimate failure strength of a lattice structure considering structural mechanics as well as fracture mechanics. To achieve the goal, we develop numerical fracture mechanic models based on the cohesive zone model. The numerical models are calibrated based on peel tests using double cantilever beam specimens. The strength degradation in material extrusion processes is assessed based on fracture toughness determined from numerical models and embedded crack length predicted from process simulation models. Figure 2 shows a conceptual diagram for the research framework.

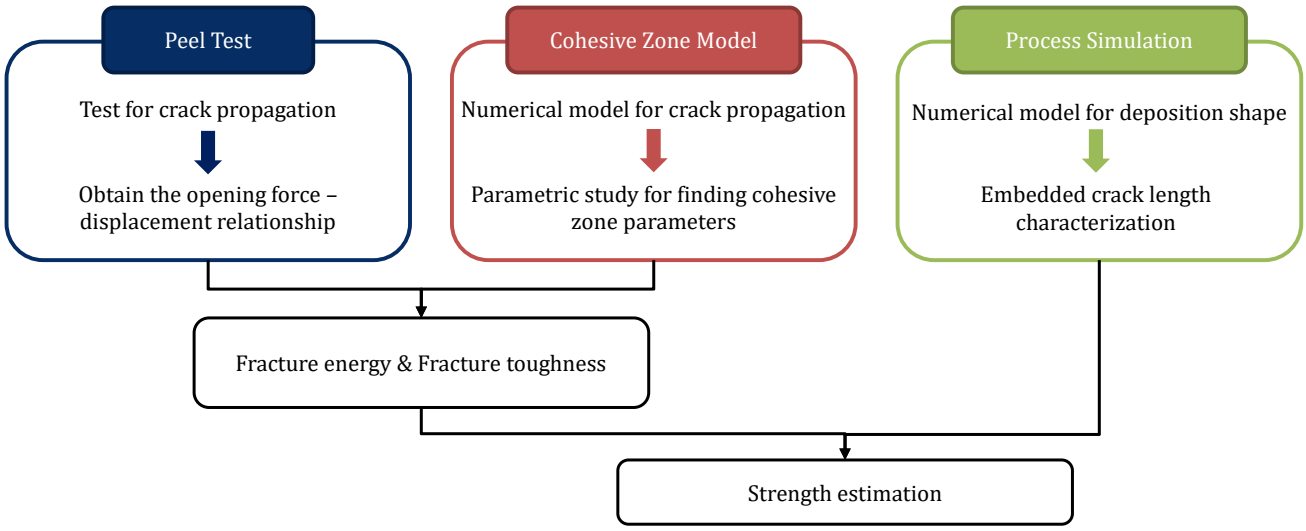

Figure 2 Conceptual diagram for research framework

In following sections, we explain an experimental procedure for a peel test, and describe a numerical modeling procedure using cohesive elements. Next, we present parametric study to calibrate cohesive parameters in the numerical model based on test results. Then, we explain a process simulation model to determine initial crack length. Finally, we present the estimation procedure and the results.

Peel Test

In this research, ASTM D5528-13 testing method is implemented to quantify mode I inter-laminar fracture toughness [18]. Figure 3 (a) shows a standard double cantilever beam specimen. The standard DCB specimen is devised to assess bonding strength of a continuous fiber-reinforced composite material. However, this DCB specimen is not suitable to measure bonding strength between deposition paths in material extrusion for two reasons. The first is that infill raster pattern is not controllable and the second is that bonding strength between two deposition paths is of interest in this work. To solve the problem, the standard specimen is modified as shown in Figure 3 (b). The modified DCB specimen has a small interlayer bonding area, which is filled with only two deposition paths so that it is guaranteed that only two deposition paths are bonded between layers.

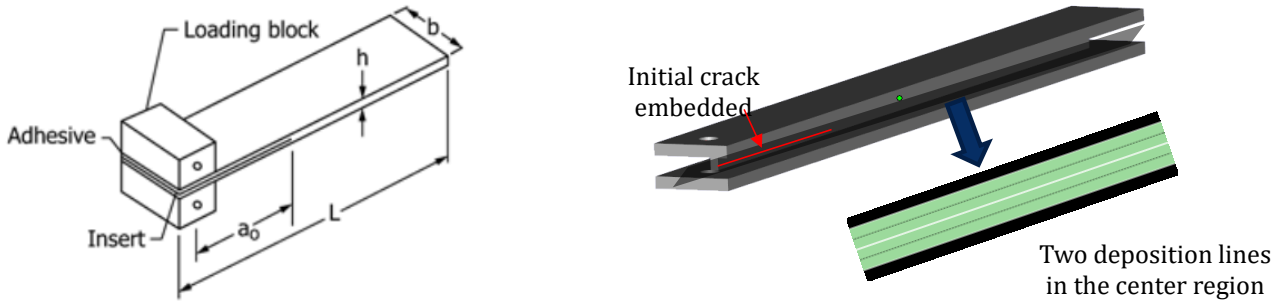

(a) Standard DCB specimen **(b) Modified DCB specimen**

Figure 3 Standard and modified peel test specimens

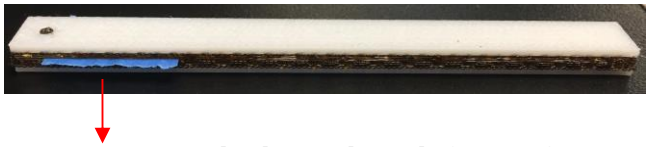

Figure 4 Fabricated DCB specimen

The specimens were fabricated in Dimension 1200se from Stratasys®. The raw material was ABS P400 and a T16 nozzle tip was used, which leads 0.254mm layer thickness. To embed an initial crack in the specimens, we paused fabrication process after deposition for the 7th layer, and we applied a strap of a 3M® blue paper masking tape to locate an initial crack. The crack length is 23 mm. After that, we resumed the process to complete fabrication. Figure 4 shows a fabricated DCB specimen. Peel tests are performed in an Instron® universal tensile test machine. The specimens were installed using metal wires as shown in Figure 7 (a).

Cohesive Zone Model

In this work, we utilize a cohesive zone model to simulate interlayer bonding fracture in DCB specimens. CZM is capable to describe a gradual separation phenomenon caused by crack growth. A traction-separation law (TSL), which defines a relationship between cracking opening and required traction characterizes this model. Several traction-separation laws have been proposed based on material characteristics. In this research, a bilinear traction-separation law shown in Figure 5 is used. In the bilinear traction-separation law, it is assumed that the relationship is composed of two linear regions. To define the two linear regions, three important parameters are required. The parameters are penalty stiffness, cohesive strength and fracture energy.

The penalty stiffness is related to an initial mechanical response of a cohesive zone before cohesive traction reaches cohesive strength. The magnitude of the penalty stiffness must be high enough to avoid interpenetration of crack surfaces [19]. In this work, the penalty stiffness is selected based on an approach proposed by Turon et al. [20] as following:

$$K = \alpha \frac{E}{t} \tag{1}$$

where, E is an elastic modulus of a raw material, t is a thickness of plies adjacent to a bonding region, and α is a parameter much larger than 1. In this work, α is set to 50, which is recommended by Turon et al.

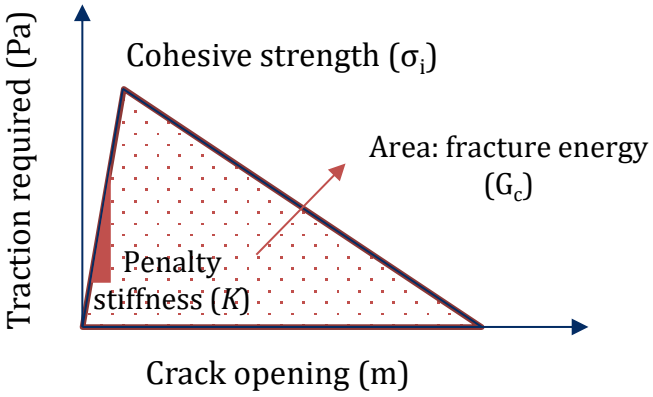

Figure 5 Bilinear traction-separation law

The cohesive strength is related to damage initiation. After cohesive traction reaches the cohesive strength, required cohesive traction starts to be reduced due to damage accumulation. There are several criteria based on stress, strain or displacement field in deformed configuration. In this work, the maximum stress criterion is used to determine damage initiation and the value of cohesive strength is set to $0.55\sigma_Y$, where σ_Y is yield strength of the raw material.

The area below a traction-separation law is a fracture energy that is directly related to fracture toughness. Once the fracture energy is determined, damage propagation response can be expressed. In this paper, we determine a value that minimizes difference in the maximum traction force between peel test and finite element analysis with CZM for the fracture energy.

Parametric Study for Calibrating Fracture Analysis

The cohesive zone model explained in the previous section is implemented to a numerical model of a DCB specimen in ABAQUS®. The numerical DCB specimen model is shown in Figure 6. A thickness of cohesive zone is set to 1 μm, and the zone is modeled using 8-node three-dimensional cohesive elements (COH3D8). The nonlinear analysis is performed using the model and results are compared with test rsults. Figure 7 shows a deformed shape of DCB specimens in the test and analysis.

To determine the fracture energy, we construct a response surface model based on results from four different fracture energy levels, which are 100, 200, 300, 400 N/m. The traction force – opening displacement responses from analysis are compared with those from peel tests in Figure 8. The smaller fracture energy is applied to the cohesive zone model, the weaker traction force is yielded in specimens. The fracture energy and fracture toughness of each specimens are determined from the response surface model as listed in Table 1. The fracture toughness obtained in this section is used to estimate fracture failure of lattice structure with initial crack length based on process simulation model in the following section.

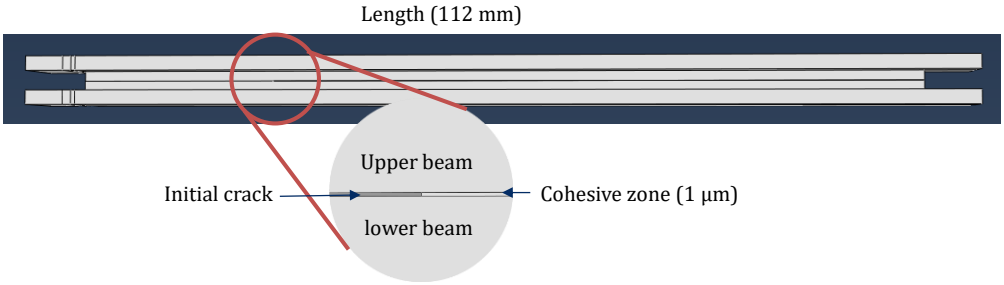

Figure 6 Cohesive zone modeling for modified DCB specimens

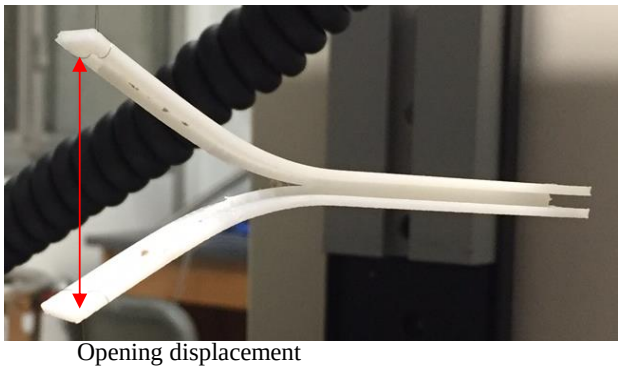

(a) Peel test

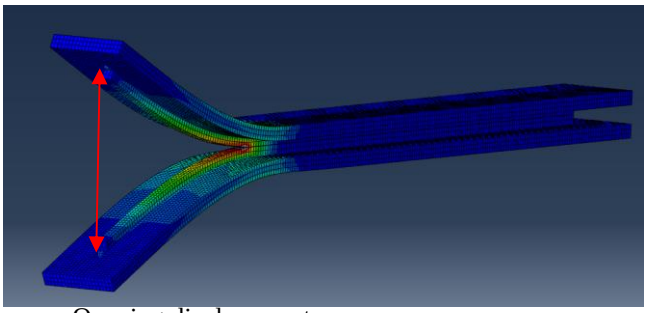

(b) Finite element analysis

Figure 7 Deformed shapes

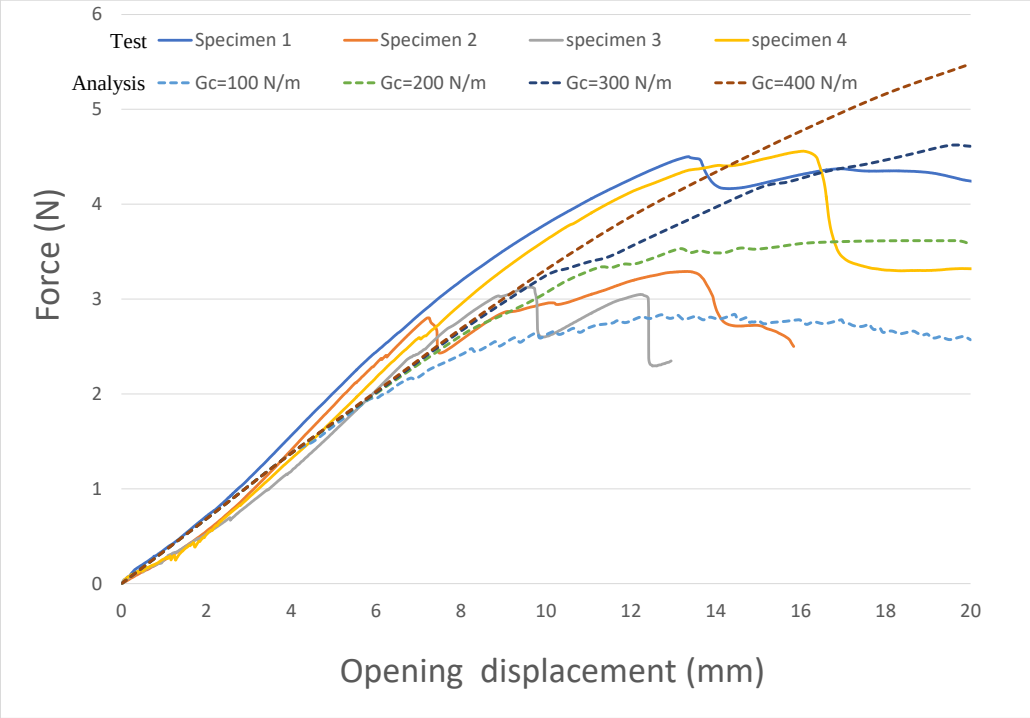

Figure 8 Comparison: Test vs Analysis

Table 1 Determined fracture toughness based on parametric study

	Specimen 1	*Specimen 2*	*Specimen 3*	*Specimen 4*	*Mean*
Fracture Energy (N/m)	290.68	100.35	136.67	297.18	206.22
Fracture toughness (MPa/√m)	0.407	0.239	0.279	0.411	0.334

Process Simulation Modeling

In this work, we utilize a process simulation modeling approach proposed by Watanabe et al. [21]. Two dimensional process simulation models for material extrusion are developed using ANSYS® Polyflow analysis package. This process simulation model is capable to describe deposition shape and temperature distribution during material extrusion. The simulation modeling is composed of two stages. The first simulation model is deposition and cooling model of the first layer of filament.

The first layer is deposited onto a build platform, which is assumed to be at a constant temperature of 100 °C. The geometry and mesh before the deposition is shown in Figure 9 (a). A volumetric flow rate at the nozzle, Q is calculated using Eqn. (2):

$$Q = v_r WH \tag{2}$$

where v_r is the deposition velocity, W is the width of the deposited road, and H is its height, assuming that the deposited filament had more of a rectangular shape than circular [22]. By applying the calculated volumetric flow rate at the nozzle entrance and gravitational force, and using the remeshing technique in ANSYS® Polyflow, the deposition of the first layer was performed.

The second simulation model was the deposition of the second layer of filament on top of the first layer. Once, the temperature distribution after the first layer cooling was exported from the previous simulation, and the geometry and mesh before the second layer deposition is shown in Figure 9 (b). The procedure for this simulation model was similar to that for the first layer deposition. However, it was crucial to simulate the conduction heat transfer between the two layers in this stage. This was accomplished using the fluid-to-fluid contact capability in ANSYS® Polyflow. Required material properties of ABS P400 are listed in Table 2.

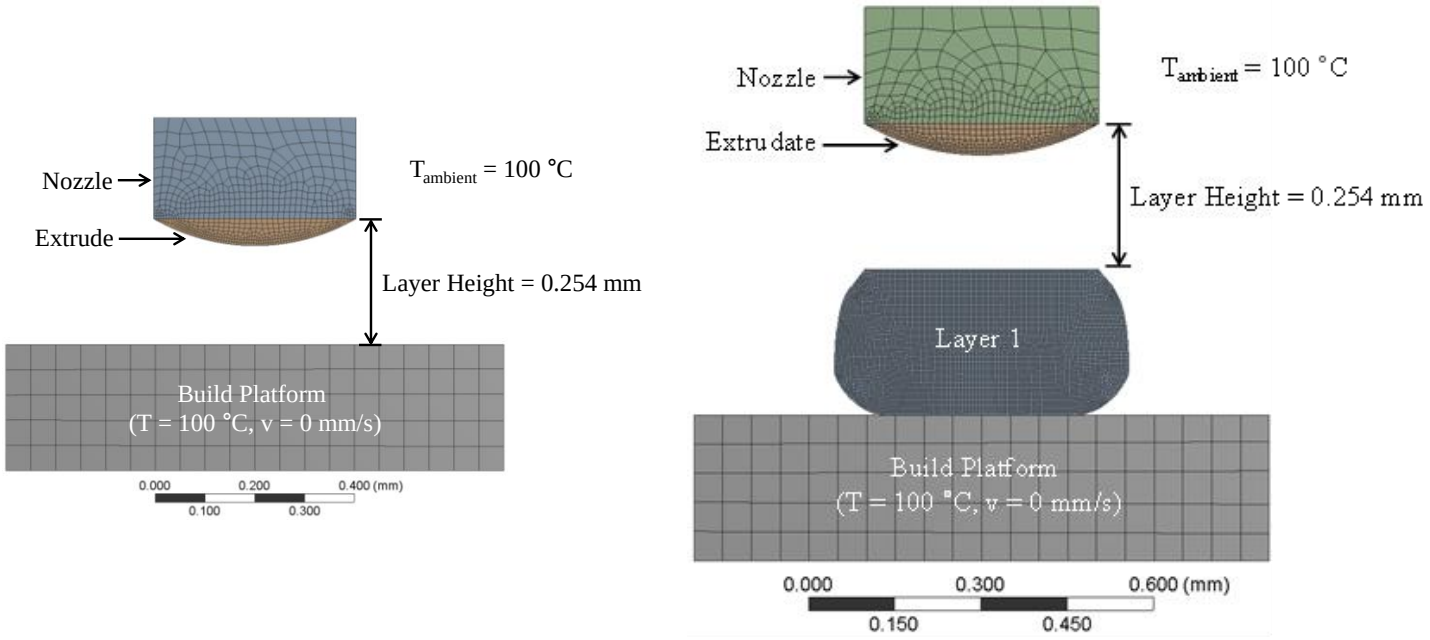

(a) 1st layer deposition **(b) 2nd layer deposition**

Figure 9 Material extrusion process simulation modeling

Table 2 Material properties of ABS

Viscosity Expression	$\eta = e^{\left[5675.2\left(\frac{1}{T}-\frac{1}{503.15}\right)\right]}22289(\dot{\gamma})^{-0.68}$
Coefficient of Thermal Expression	7.38 x 10-5 m/(m-°C)
Thermal Conductivity	0.17 W/(m-°C)
Specific Heat	1423.51 J/(kg-°C)
Density	1040 kg/m3
Glass Transition Temperature (Tg)	105.0 °C

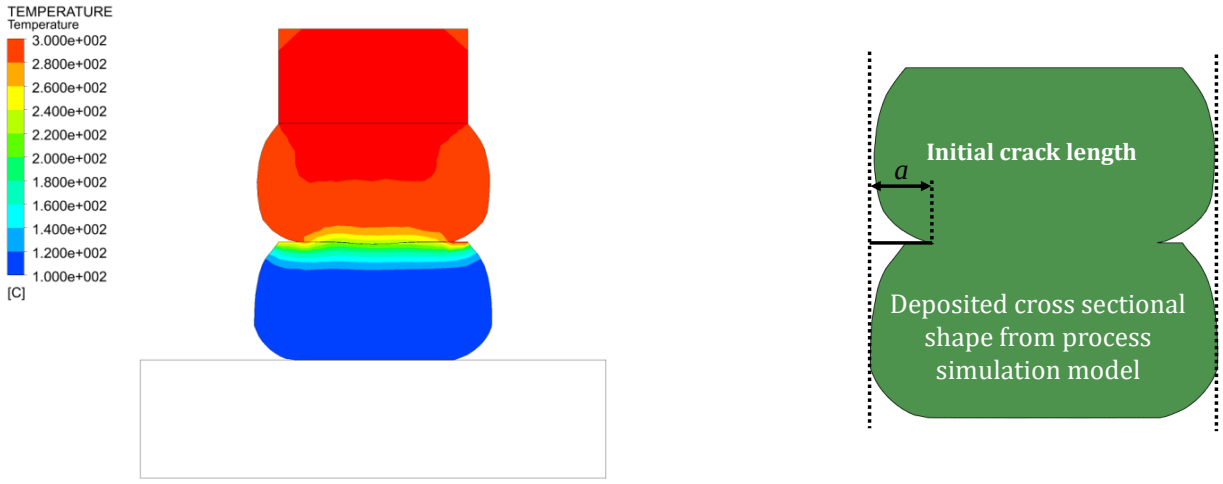

(a) Deposited shape and temperature distribution **(b) Embeded crack length**

Figure 10 Resulting shape and temperature distribution

Figure 10 (a) shows resulting deposition shape and temperature distribution. The crack length between layers is measured as shown in Figure 10 (b). The measured initial crack length is 0.08532 mm. This crack length is incorporated into fracture failure criteria in the following section.

Estimation of Strength of Lattice Structure

In this section, a failure criterion of lattice structures considering fracture is developed and presented. Mechanical properties of lattice structures depend on their microscopic characteristics. Once a strut in a lattice structure starts to fail, the lattice structure also starts to fail. Two failure modes are considered in this research. The first is elastic failure and the other is fracture failure. The conceptual description of failure criteria is presented in Figure 11.

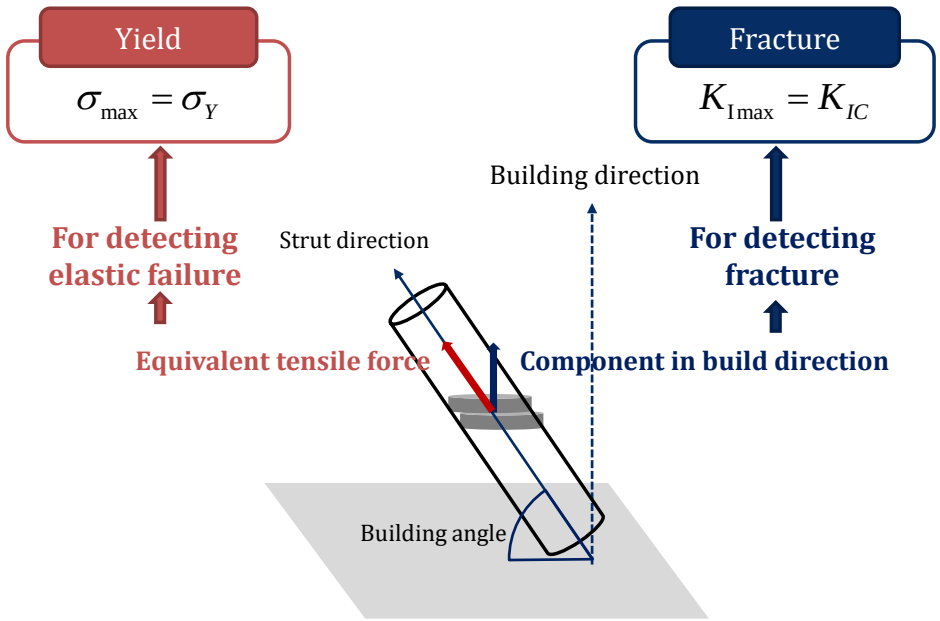

Figure 11 Failure criteria of a strut in a lattice structure

In this work, the elastic failure criterion is developed based on yielding of a strut. For detecting elastic failure, resultant axial stress by external forces is compared with yield strength of a raw material, which is 22 MPa for ABS P400. It is noteworthy that the total axial force is considered for elastic failure. The fracture failure criterion is established by utilizing fracture toughness of a cracked cylinder. A strut in a lattice structure is considered as a cracked cylinder. It is assumed that the cracked cylinder is fractured when resultant stress intensity factor reaches the fracture toughness. The stress intensity factor is calculated based on Gao and Herrmann's work [23] as following:

$$K_{I\max} = \sigma_{\max}\sqrt{\frac{\pi^2 r}{2}\left(\frac{I}{I_c}-1\right)} \qquad I = \frac{\pi r^4}{4}, \quad I_c = I\left(1-\frac{a^4}{r^4}\right) \tag{3}$$

where, $K_{I\max}$ is the maximum resultant stress intensity factor, $\sigma_{\max}$ is maximum resultant axial stress, r is the radius of strut, and a is the embedded crack length. To calculate the stress intensity factor of a strut using Eqn. (3), the crack length is required. In this work, the crack length determined in the previous section is applied. For detecting fracture failure, only force component in the building direction is applied to calculate stress intensity factor. The fracture toughness for this criterion is set to calculated fracture toughness with the CZM model in the previous section.

Figure 12 shows a tensile specimen for validating the proposed estimation approach. The specimen has 2D rectangular lattice structures in the center. Tensile specimens are fabricated in Dimension® 1200es with the same process parameters for DCB specimens at five different building angles: 0°, 30°, 45°, 60°, 90°. The fabricated specimens are tested in the Instron universal tensile test machine.

Figure 13 presents comparison among estimation and experimental results. The experimental result shows significant drop in strength when the specimens are built at high building angles. However, elastic failure criterion is not able to capture this strength degradation since the main failure mode of specimens built at high angle is fracture. The fracture criterion improves estimation by describing fracture mode failure.

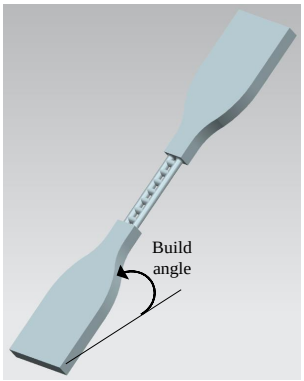

Figure 12 Tensile specimen with 2D rectangular lattice structure

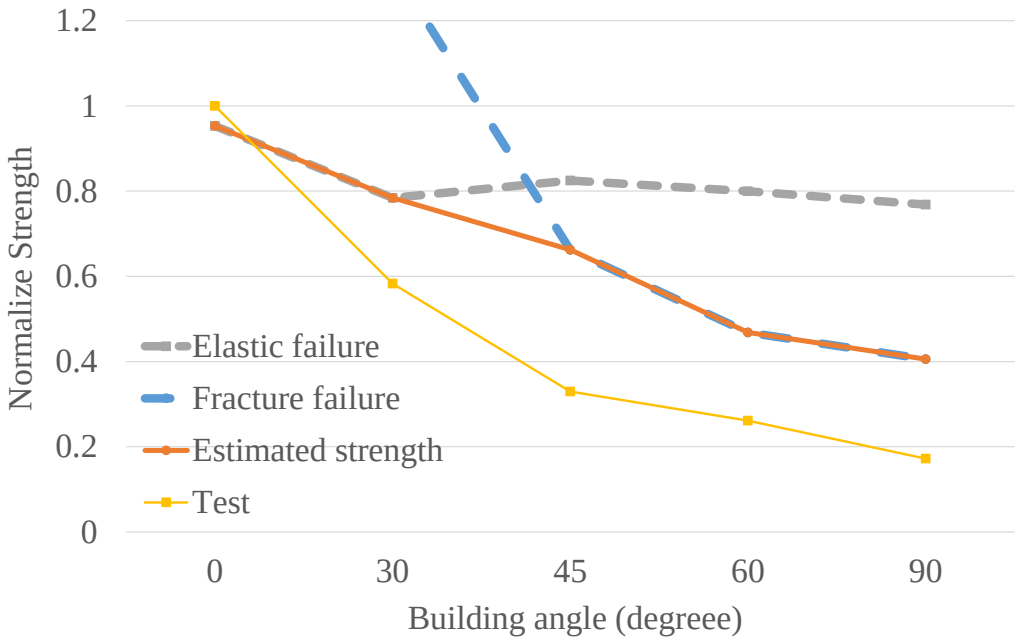

Figure 13 Comparison of estimated strength of 2D rectangular lattice structure

Estimation of Strength of Lattice Structure using Cohesive Zone Model

In this section, strength of tensile test specimens with two dimensional rectangular lattice structures is estimated using cohesive zone model developed in previous sections. Numerical models of the specimens at 0° and 90° building angles are modeled using an as-fabricated voxel modeling approach as shown in Figure 14. Using symmetricity, half of a rectangle is generated. A layer of cohesive elements is inserted between layers near a joint. The obtained cohesive parameters in the previous section are implemented to the cohesive elements.

Comparison of normalized strength among estimates and measurements are listed in Table 3. At the zero building angle specimen which is built horizontally parallel to building plane, estimates using Eqn. (3) is similar to the cohesive zone model as shown less than 10% error. However, at the 90° degree building angle, estimates using Eqn. (3) shows large error over 130% larger than the experiment measurement.

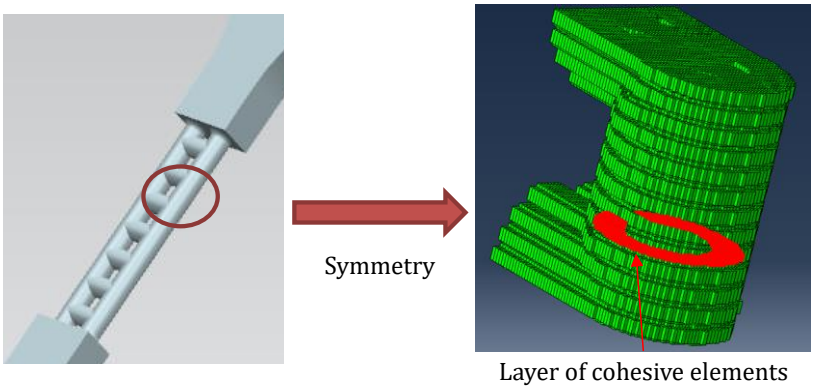

Figure 14 As-fabricated voxel model with cohesive elements

Table 3 Comparison of normalized strength

Building angle	*0°*	*90°*
Estimated strength using Eqn. (3)	**0.953 (-4.69%)**	**0.406 (135.56%)**
Cohesive zone model	**0.914 (-8.58%)**	**0.160 (-7.36%)**
Experiment	**1.000**	**0.172**

Conclusion

This research proposes a strength-estimation approach for a lattice structure considering interlayer fracture. We developed a numerical model for a double cantilever beam specimen with cohesive elements and determined the cohesive parameters by comparing mechanical responses with experimental results. The embedded crack length between layers was determined by process simulation model. The estimates for strength of a lattice structure were calculated analytically and numerically. For analytic approach, the stress intensity factor of a strut with calculated crack length was compared with fracture toughness from numerical analysis of double cantilever beam models. For numerical approach, strength of a lattice structure was determined from the maximum force of an as-fabricated voxel model with cohesive elements. Comparison found that significant strength degradation at high building angles can be predicted by considering interlayer fracture phenomenon, and that the proposed approach using the cohesive zone model is capable of capturing interlayer fracture mode and improving accuracy of the strength-estimation procedure. In the future research, we will investigate more lattice structures using the proposed approach.

Acknowledgement

The authors gratefully acknowledge support from the National Science Foundation, grants CMMI-1200758 and CMMI-1538744. Any opinions, findings, and conclusions or recommendations expressed in this publication are those of the authors and do not necessarily reflect the views of the National Science Foundation.

Reference

1. Ahn, D., Kweon, J.-H., Kwon, S., Song, J., and Lee, S., *Representation of surface roughness in fused deposition modeling.* Journal of Materials Processing Technology, 2009. **209**(15): p. 5593-5600.
2. Karamooz Ravari, M.R., Kadkhodaei, M., Badrossamay, M., and Rezaei, R., *Numerical investigation on mechanical properties of cellular lattice structures fabricated by fused deposition modeling.* International Journal of Mechanical Sciences, 2014. **88**: p. 154-161.
3. Harrysson, O.L.A., Cansizoglu, O., Marcellin-Little, D.J., Cormier, D.R., and West, H.A., *Direct metal fabrication of titanium implants with tailored materials and mechanical properties using electron beam melting technology.* Materials Science and Engineering: C, 2008. **28**(3): p. 366-373.
4. Ahn, S.H., Montero, M., Odell, D., Roundy, S., and Wright, P.K., *Anisotropic material properties of fused deposition modeling ABS.* Rapid Prototyping Journal, 2002. **8**(4): p. 248-257.
5. Rodríguez, J.F., Thomas, J.P., and Renaud, J.E., *Design of fused-deposition ABS components for stiffness and strength.* Journal of Mechanical Design, 2003. **125**(3): p. 545-551.
6. Bagsik, A., Schöppner, V., and Klemp, E. *FDM part quality manufactured with Ultem* 9085*. in *14th international scientific conference on polymeric materials*. 2010.
7. Thomas, J. and Rodríguez, J. *Modeling the fracture strength between fused deposition extruded roads*. in *Proceedings of the 11th Solid Freeform Fabrication Symposium*. 2000.

8. Young, D., Kessler, J., and Czabaj, M. *Interlayer fracture toughness of additively manufactured unreinforced and carbon-fiber-reinforced acrylonitrile butadiene styrene*. in *Proceedings of the American Society for Composites - 31st Technical Conference, ASC 2016*. 2016.
9. Gardan, J., Makke, A., and Recho, N., *A Method to Improve the Fracture Toughness Using 3D Printing by Extrusion Deposition.* Procedia Structural Integrity, 2016. **2**: p. 144-151.
10. Kishore, V., Ajinjeru, C., Nycz, A., Post, B., Lindahl, J., Kunc, V., and Duty, C., *Infrared preheating to improve interlayer strength of big area additive manufacturing (BAAM) components.* Additive Manufacturing, 2017. **14**: p. 7-12.
11. Seppala, J.E., Hoon Han, S., Hillgartner, K.E., Davis, C.S., and Migler, K.B., *Weld formation during material extrusion additive manufacturing.* Soft Matter, 2017.
12. Alfano, M., Furgiuele, F., Leonardi, A., Maletta, C., and Paulino, G.H. *Cohesive zone modeling of mode I fracture in adhesive bonded joints*. in *Key Engineering Materials*. 2007. Trans Tech Publ.
13. Campilho, R.D.S.G., de Moura, M.F.S.F., and Domingues, J.J.M.S., *Using a cohesive damage model to predict the tensile behaviour of CFRP single-strap repairs.* International Journal of Solids and Structures, 2008. **45**(5): p. 1497-1512.
14. Park, K., Choi, H., and Paulino, G.H., *Assessment of cohesive traction-separation relationships in ABAQUS: A comparative study.* Mechanics Research Communications, 2016. **78, Part B**: p. 71-78.
15. Liravi, F., Das, S., and Zhou, C., *Separation force analysis and prediction based on cohesive element model for constrained-surface Stereolithography processes.* Computer-Aided Design, 2015. **69**: p. 134-142.
16. Spackman, C.C., Nowak, J.F., Mills, K., and Samuel, J., *A cohesive zone model for the stamping process encountered during 3d printing of fiber-reinforced soft composites.* Journal of Manufacturing Science and Engineering, 2017.
17. Ahmadi, A., Mirzaeifar, R., Moghaddam, N.S., Turabi, A.S., Karaca, H.E., and Elahinia, M., *Effect of manufacturing parameters on mechanical properties of 316L stainless steel parts fabricated by selective laser melting: A computational framework.* Materials & Design, 2016. **112**: p. 328-338.
18. *Standard Test Method for Mode I Interlaminar Fracture Toughness of Unidirectional Fiber-Reinforced Polymer Matrix Composites*. 2013, ASTM International.
19. Moslemi, M. and Khoshravan, M., *Cohesive zone parameters selection for mode-I prediction of interfacial delamination.* Strojniški vestnik-Journal of Mechanical Engineering, 2015. **61**(9): p. 507-516.
20. Turon, A., Dávila, C.G., Camanho, P.P., and Costa, J., *An engineering solution for mesh size effects in the simulation of delamination using cohesive zone models.* Engineering Fracture Mechanics, 2007. **74**(10): p. 1665-1682.
21. Watanabe, N., Shofner, M., Treat, N., and Rosen, D. *A model for residual stress and part warpage prediction in material extrusion with application to polypropylene*. in *2016 Annual International Solid Freeform Fabrication Symposium*. 2016.
22. Mukesh, K.A., Vikram, R.J., Noshir, A.L., Ahmad, S., Philip, J.W., and Stephen, C.D., *Structural quality of parts processed by fused deposition.* Rapid Prototyping Journal, 1996. **2**(4): p. 4-19.
23. Huajian, G. and Herrmann, G., *On estimates of stress intensity factors for cracked beams and pipes.* Engineering Fracture Mechanics, 1992. **41**(5): p. 695-706.